In-vitro Bubble-Enhanced Heating for Focused Ultrasound Treatments in the Brain

Department of Bioengineering

June 2020

Sierra Bonilla
Averkiou Lab
Mike Averkiou, Associate Professor of Bioengineering
Alicia Clark & Dingjie Suo

Abstract

High Intensity Focused Ultrasound (HIFU) is a noninvasive treatment clinically used to ablate targeted tissues in the brain, like for essential tremors. For HIFU brain treatments, a large amount of energy is absorbed and reflected by the skull making targeting more difficult when desired target regions are near the skull. Ultrasound contrast agents are 1-10 μm inert gas bubbles commonly used to enhance the contrast in ultrasound images. Current research on the use of HIFU treatment in conjunction with ultrasound contrast agents, referred to as bubble-enhanced heating (BEH), is being performed due to certain contrast agent's ability to convert acoustic energy into heat more efficiently through thermal, viscous, and acoustic damping. There is a need to study acoustic pressures and microbubble concentrations in image-guided bubble enhanced heating. The goal of this project is to develop a tissue-mimicking phantom with similar acoustic properties to human tissue and design an appropriate experimental setup to perform *in-vitro* HIFU heating experiments. These results will help aid the development of bubble-enhanced heating as the next step in focused ultrasound neurological treatments.

Table of Contents

Introduction **3**
1. **Project Definition** **3**
2. **Significance** **3**
   2.1 Essential Tremors 3
   2.2 Statement of Problem & Need 4
   2.3 Impact 4
3. **Social, Ethical, Regulatory, and Economic Issues** **5**
4. **Technical Background** **5**
   4.1 Focused Ultrasound Surgery 5
   4.2 Ultrasound Contrast Agents 7
   4.3 Tissue-Mimicking Phantoms 8
5. **Engineering Standards & Current Technologies** **8**
6. **Previous Relevant Work from the Averkiou Research Group** **9**
7. **Outstanding Technical Issues & COVID-19 Impact** **10**

Experiments **11**
1. **Design & Research Plan** **11**
2. **Materials** **13**
3. **Methods: Development of the *In-Vitro* Research Platform** **14**
   3.1 Phantom Characterization 14
   3.2 Microbubble Dilution 18
   3.3 Temperature Measurement Method 20

Results **23**
1. **Final *In-Vitro* Research Platform Design & Experimental Protocols** **23**
2. **Temperature & Imaging Results** **26**

Discussion **29**
1. **Analysis & Conclusions** **29**
2. **Future Work** **31**

Acknowledgements **33**

References **34**

Introduction

1. Project Definition

Bone is highly reflective and absorptive which limits the transmissivity of acoustic waves. Since high intensity focused ultrasound (HIFU) relies on depositing large amounts of acoustic energy, it is quite difficult to treat neurological disorders using focused ultrasound because of the barrier of the skull, when the target region is near the skull. The problem stems from the inability to deposit enough acoustic energy to heat up and destroy a targeted location, while keeping the pressures low enough to not cause harm to healthy tissues or cause excess heating at the transducer contact point. Currently, focused ultrasound is only capable of safely targeting minute regions at the center of the brain, like in essential tremors where the dysfunctional neural network is located in the thalamus[41]. Safely increasing the ablation zone and increasing feasible target regions to treat a wider range of neurological disorders is the next step in focused ultrasound neurological treatments. Contrast agents, specifically microbubbles, have been shown to enhance the therapeutic ability of ultrasound through mechanical and thermal mechanisms seen in applications like opening the blood brain barrier (BBB) and drug delivery[41],[42].

Our solution proposes using this technology to enhance the HIFU thermal effect through treating using HIFU in conjunction with microbubbles, referred to here as bubble-enhanced heating (BEH). The research developed in my capstone focuses on developing a research platform to study image-guided, reproducible microbubble temperature enhancement in an *in-vitro* model. Through this research we hope to determine the ideal pressures and microbubble concentrations to treat a wider range of neurological disorders safely and effectively.

Insightec was a key partner in this project. Insightec is a medical device company developing MR guided Focused Ultrasound equipment. Recommending standardized concentrations and acoustic pressures based off results produced in this work will help Insightec further develop MR guided Focused Ultrasound treatments [43].

2. Significance

2.1 Essential Tremors

According to the Focused Ultrasound Foundation, essential tremors are the most common movement disease and affect 3% of the U.S. population [5]. Essential tremors are characterized by significant shaking of the hands and can impair one's ability to perform daily activities. It is caused by dysfunctions in neural networks in the motor regions of the brain resulting in misfiring action tremors. These tremors are cyclic, usually ranging between 4 Hz – 12 Hz (4 to 12 cycles per second). Advances in essential tremor research

suggests that there are underlying, non-motor symptoms of essential tremors, which include cognitive impairments, sleep disorders, anxiety, and other neurological disorders [9]. Due to its complexity, essential tremors are categorized as a family of diseases which renders it quite difficult to treat. Current treatments include beta blockers, anti-seizure medications, and Botox injections. These treatments focus on controlling the symptoms, but don't remove the dysfunctional neural network. Focused ultrasound treatment was FDA approved in 2016 as a method to ablate small regions of the brain known to produce essential tremors [6]. This procedure doesn't require anesthesia or incisions and enables the patient to return to daily activities quickly (usually the same day). One device, ExAblate Neuro, is currently available to perform this MR-guided focused ultrasound therapy procedure [43].

2.2 Statement of Problem & Need

This project is defined by the need to treat a wider range of neurological disorders using focused ultrasound due to its preferential non-invasive characteristics. The problem is that using focused ultrasound requires high power output and can lead to adverse side effects when the target region is near the skull. Additionally, focused ultrasound treatments in the brain require a lower frequency transducer than other focused ultrasound treatments because of the attenuation from the skull. Since this is a newer technology, there is no standardized protocol for BEH. For BEH to be a clinical therapy, bubble nucleation and activity must be extensively studied and shown to reproducibly form lesions through well understood mechanisms [21]. So, the objective of this work was to develop a platform to study *in-vitro*, image-guided bubble-enhanced heating to recommend microbubble concentrations and acoustic pressures for *in-vivo* brain treatments.

2.3 Impact

Developing recommendations for microbubble concentrations and acoustic pressures will have impacts in both research and the clinic. Future work can be done by building on these optimal recommendations to create a standardized protocol for BEH, so that *in-vivo* experiments are better informed. Also, the creation of a platform to study *in-vitro*, image-guided bubble enhanced heating will allow for future studies beyond the ones completed in this capstone. Other research groups can compare their work to that completed here to help design their research plans. Overall, the impact of this project will be to recommend image-guidance procedures, microbubble concentrations, and acoustic pressures to perform *in-vitro* BEH experiments to aid the development of focused ultrasound neurological treatments.

3. Social, Ethical, Regulatory, and Economic Issues

This technology has significant social considerations associated with it due to its therapeutic translation. Although ultrasound is noninvasive, this technology permanently ablates a lesion into the brain and has side effects and risks. Patient preference and involvement is important to study, since the choice to undergo focused ultrasound therapy will be an autonomous medical decision. Ablating tissue non-invasively sounds intimidating and will require extensive communication using appropriate, non-technical language. The patient must be aware of adverse risks and be tolerant of the therapy type. This research didn't include any animal studies, but future work may. This future work will follow the Guidelines for Ethical Conduct in the Care and Use of Animals provided by American Association of Psychologists [27].

Despite the advantages of this technology, economic limitations remain. This technology, if available clinically, would be much more expensive than alternative treatments (medications, RF ablation, etc.). To perform focused ultrasound surgery, currently a magnetic resonance imaging machine is required for real-time imaging to receive temperature measurements and localize and target treatment zones. There is only one current MR guided focused ultrasound system available on the market. The system is expensive and is not available at every hospital. However, if in the future ultrasound is used as the method to guide treatment, like seen in this report, the cost of the procedure would be considerably lower.

4. Technical Background

4.1 Focused Ultrasound Surgery

According to global statistics, cancer is the second leading cause of death worldwide [1]. Current common treatments include radiotherapy, surgery, and chemotherapy. These treatments tend to damage healthy cells when destroying or removing the cancerous cells, resulting in many side effects like hair loss, neutropenia, and/or lymphedema [2]. Image-guided focused ultrasound surgery is a quickly developing technology that has increased in popularity over the last 20 years. It has a broad spectrum of potential applications including tumor ablation [45]. Focused ultrasound surgery uses high intensity focused ultrasound (HIFU), a non-invasive treatment that utilizes highly focused ultrasonic beams to deposit acoustic energy to a targeted tissue. HIFU has been used in clinics around the world to treat a variety of malignant tumors and is FDA approved to treat pancreatic tissue, uterine fibroids, and essential tremors [3]. Unlike common cancer treatments, HIFU is noninvasive, non-radiating, and produces fewer side effects. Along with tumor treatment, HIFU has been evaluated for palliative treatment in pancreatic cancer. The prognosis for patients with pancreatic cancer is one of the worst compared with all other types of cancer and high levels of pain is often reported [7]. A study at the University of Washington found a

substantial reduction in pancreatic tumor related pain with very few side effects following HIFU treatment [8]. Because of the desirable characteristics of HIFU treatment, a range of clinical applications such as neurosurgery, ophthalmology, urology, and more are being explored [3].

It works like a magnifying glass with the sun, but instead of optical waves, HIFU uses sound waves (Figure 1). The ultrasound beam is focused by a physical lens in a single element transducer or by timed element beamforming in an array transducer. The sound wave propagates through body and at the specified focal point inside the body, the waves sum to have the greatest amplitude (Figure 2).

Figure 1: This Figure was adapted from lumenlearning to show the sound energy focused by a lens to a focal point [47].

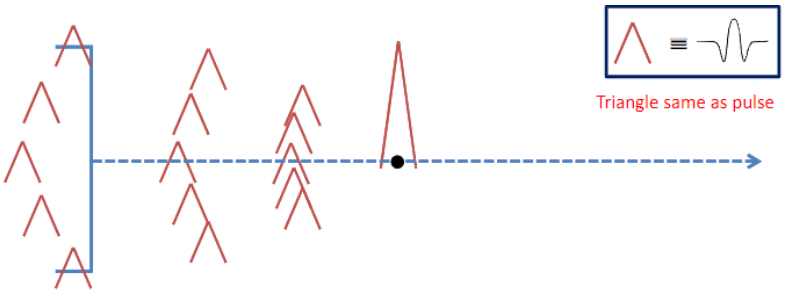

Figure 2: This Figure was taken from a lecture given by Dr. Averkiou. A focused ultrasound beam is transmitted on the left (from the face of the transducer). When the pulses arrive at the focal spot (the black dot), they sum to the greatest amplitude.

This energy is converted to thermal energy and can raise the tissue temperature to 60-95 °C, resulting in localized tissue necrosis and ablation [19]. At higher acoustic powers, a larger, migrating protein coagulation site is produced thus stressing the importance of HIFU characterization to avoid unwanted tissue damage [13]. Although HIFU is currently used in clinics for certain tissue ablation therapies, the efficiency and safety of the technology decreases when the targeted tissue region is large and near high-speed blood flow due to increased acoustic attenuation. To address these problems, many groups have studied HIFU in conjunction with a variety of gas-filled micro and nanobubbles. These studies show greater ablation zones are created with these bubbles and the treatment requires shorter acoustic exposures and lower acoustic pressures [10], [20]. Additionally, a major impediment with treating deep seated solid tumors with HIFU is the long treatment times as well as unwanted tissue damage due to the high ultrasound intensities used in treatments.

4.2 Ultrasound Contrast Agents

In ultrasound, images are created by sending acoustic waves into the body using a transducer and the body's tissues reflect sound back. The transducer listens to the reflected sound and the ultrasound system processes the received signals to produce an image. Blood is a weak scatterer of sound, making it difficult to visualize the vasculature. So, contrast agents can be introduced to the blood stream to image the vasculature in detail. Contrast agents are stabilized inert gas microbubbles, approximately the size of a red blood cell (1-10 μm). Clinically, microbubbles are used to improve the image quality and visualize the vasculature using ultrasound [14]. Under acoustic wave pressures, microbubbles undergo volumetric changes that result in mechanical movements [12]. This mechanical action has been shown to enhance the therapeutic ability of ultrasound. The microbubble undergoes a frequency and pressure dependent volumetric oscillation. As the frequency gets closer to the bubble's resonant frequency, the bubble increases in proportional volumetric changes, called cavitation. There are two main types of cavitation, stable and inertial. Stable cavitation occurs when microbubbles are forced to oscillate with small deformations in a relatively low amplitude pressure field. When microbubbles are exposed to a high intensity acoustic field, the bubbles will grow in volume and then collapse violently. This is referred to as inertial cavitation. The mechanical index, a common measurement of pressure, is used to describe microbubble activity thresholds. The mechanical index (MI) is equal to the pressure of the acoustic field divided by the center frequency:

$$MI = \frac{P_-}{\sqrt{f_c}}$$

A mechanical index of 0.1 is considered low, 0.2-0.7 is considered moderate, and above 0.8 is high. The FDA regulatory limit for ultrasound imaging is 1.9 MI to avoid harming the patient [44]. Between 0.05 and 0.1 MI, microbubbles undergo stable cavitation and above 0.5 MI, microbubbles are known to cavitate inertially. Another intriguing property of microbubbles, that of their ability to transform energy from one state to another, was discussed in Coussios and Roy's review of bubble fluid mechanics. They showed that bubble oscillations do work on the surrounding fluid, dissipating as viscous heating and sound radiation [11].

Microbubbles have been shown to have desirable physical attributes, like that of dissipation of viscous heating and implosive collapsing, that are currently being studied for therapeutic and diagnostic ultrasound. For example, microforces produced by acoustically excited microbubbles can increase the permeability of surrounding cell membranes, thus rendering microbubbles capable of enhancing drug delivery [18]. Lipsman et al used

microbubbles to aid drug delivery in the brain. This work utilized low-intensity MR-guided focused ultrasound to open the blood-brain barrier [42]. Another group studied various acoustic pressures (0.75 MPa to 4.5 MPa) and frequencies (1.5 to 8 Hz) to determine the ideal mechanical index, 0.25, to produce microbubble vaporization or cavitation [16]. Microbubbles are currently being used in research and clinically in cardiology and radiology for both therapeutic and diagnostic applications. Although microbubbles have great feasibility for therapeutic use, bubble mechanisms and physics are complicated and need to be properly studied prior to clinical translation.

4.3 Tissue-Mimicking Phantoms

In medical imaging, phantoms are specimens of known material properties and geometries that are used to characterize or study imaging systems [46]. A tissue-mimicking phantom for ultrasound research emulates specific acoustic properties of biological tissue and is commonly used to study therapeutic ultrasound and other *in-vitro* research [23]. Several phantoms have been shown in literature to simulate ultrasound induced thermal lesion formations. One study used red blood cells suspended in agarose gel to mimic soft tissue and studied the phantom's response to cavitation using short HIFU pulses. The HIFU induced lesions were visualized clearly due to red blood cell rupturing [23]. Due to limited access to human proteins, most studies use animal derived protein bases for their phantoms like bovine serum albumin (BSA) and egg-whites. Many of these proteins are temperature-sensitive indicators, coagulating at ~60°C (similar to human tissue) [17], [13]. During phantom fabrication, contrast agents can be introduced to the mixture such that they are suspended equally throughout the medium [15].

5. Engineering Standards & Current Technologies

Since this technology is relatively new, none of the standards sites provide regulations or standards on HIFU treatment devices. According to the FDA and the IEEE as of 2009, there were no recognized standards or guidelines for HIFU review testing [26]. Since then the International Electrotechnical Commission (IEC) has released specifications of the ultrasound field used in medical ultrasound therapy [28]. It addresses the requirements for measurement standards of high intensity therapeutic ultrasound. Unfortunately, the website requires payment to see these requirements, so this was all the information available, in terms of engineering standards for therapeutic ultrasound. For imaging, the FDA requires lower than 1.9 MI and the real-time image guidance used in this work follows this standard [44]. For focused ultrasound to be approved by the FDA, pre-clinical and clinical trials must be submitted as evidence. The pre-clinical trials are mostly comprised of research performed at a funded laboratory site, focused on studying the "ultrasound power measurements and field characterization, in vitro and in vivo temperature measurements, thermal computational modeling, and demonstrating the

accuracy for targeting the region of interest and monitoring treatment progress" [26]. The FDA requires this before considering protocols for clinical trials.

In 2016, the FDA approved a device to treat essential tremors using MR-guided focused ultrasound. This device, ExAblate Neuro, targets and destroys specific areas in the brain associated with causing tremors [6]. ExAblate Neuro was developed by Insightec. Once they have more knowledge on the efficacy and process for bubble-enhanced heating, Insightec will be able to go through the regulatory process using our research as the pre-clinical data.

Additionally, There are three FDA approved clinical microbubbles used for contrast enhancement: Optison™ (Mallinckrodt, San Diego, CA, USA), Definity® (DuPont Pharmaceuticals Co., North Billerica, MA, USA), and SonoVue® (Bracco Diagnostics, Monroe Township, NJ, USA) [29]. They are currently approved for cardiac imaging and characterizing indeterminate liver lesion in the United States.

6. Previous Relevant Work from the Averkiou Research Group

In-vivo perfusion changes caused by microbubble activity was studied by Averkiou et al. This work explored the fine balance between microbubble cavitation resulting in local perfusion increases and inertial cavitation resulting in local perfusion shutdown. The effects of pulse length and pressure amplitude on the perfusion of pig liver were measured to quantify the relative vessel perforation and extravasation. This work showed that microbubble oscillations altered the local cell permeability. They also developed ideal microbubble handling, activation, and administration procedures which will be used in my capstone work. Averkiou et al. showed the importance of avoiding high pressures to cause unwanted inertial cavitation which could lead to unwanted tissue damage in my experiments [24].

To optimize microbubble-aided drug delivery and limit cellular waste, Keller, Bruce, and Averkiou studied microbubble activity with a variety of ultrasound parameters and microbubble concentrations. The goal of the study was to determine the ideal acoustic parameters that lead to effective sonoporation while minimizing microbubble effect on cell viability. The conditions that were tested include pressures 125 kPa–1 MPa, cycles 20-1000, and concentrations 10,000–10,000,000 [10M] MBs/mL with a single element 1 MHz transducer. To measure the bubble activity ultrafast imaging was used before and after insonifying and attenuation was measured for each of the microbubble concentrations chosen. Two types of microbubbles were compared, one in-house custom and one clinical. As would be expected, the study found that with increasing microbubble concentration, attenuation increased, and at the highest concentrations the elimination zone decreased through the enclosure. The clinical bubbles showed a larger attenuation rate than the custom bubbles. The study also showed that the acoustic pressure was more influential to

bubble destruction/activity than the number of cycles. The number of cycles increased microbubble movement around the enclosure but not nucleation. At higher concentrations, not only was there attenuation, but also there were extreme acoustic pressure losses which is the most relevant finding for this work. Another relevant finding was that at higher pressures, more attenuation was found to have occurred due to the dramatic radius increase of the bubbles and an increase of non-linear sound propagated near the cell layer. Thanks to Keller, Bruce, and Averkiou, better delineation between microbubble oscillations, nucleation, and gas movement is possible for my experiments where it was ideal to focus on one microbubble process [14].

Conner Pitts, a previous member in Averkiou lab, did his capstone project on BEH as well and was instrumental in the shaping of this work. Pitts created tools to simulate the pressure field and temperature rise in a variety of mediums and with a range of acoustic parameters. These theoretical simulations will be used in conjunction with my tissue-mimicking phantom experiments. His work also includes measuring the temperature field of ultrasound propagation through glycerin and glycerin mixes (50% water). He has laid the framework for showing heat rise through simulation versus experiment.

7. Outstanding Technical Issues & COVID-19 Impact

Although higher temperatures are reached when microbubbles are present, it is not well understood how much of this effect is due to bubble stable cavitation versus inertial cavitation [22]. With the model that is set up in this report, the temperature rise can be measured and visualization of the formation of lesions can be documented. However, there is not a method presented here for which to delineate between stable versus inertial cavitation. Additionally, measuring the temperature rise inside the phantom with the resources available proved difficult. The main issue coming from avoiding changes to the temperature read-outs because of the temperature measurement device itself. We had hoped to use two thermocouples to limit this problem but didn't end up getting to this. Other work suggests that you can minimize the effect of the thermocouple by limiting its diameter to less than five times the wavelength of the ultrasound beam, which we did. However, to avoid the problem all together, we could have placed a thermocouple off the axis of the transducer by a few mm and used theory to predict the temperature rise at the focus.

Originally, this work included three aims: development of the research platform, in-vitro parametric study, and an *ex-vivo* pig liver parametric study. Because of COVID-19, the Averkiou lab was shut down from March until June 2020 and the *ex-vivo* experiments were not completed. The *ex-vivo* pig liver work was completely left out in the description of this project.

Experiments

1. Design & Research Plan

To study the effects of HIFU in conjunction with microbubbles *in-vitro*, a tissue-mimicking phantom was designed and constructed for BEH experiments. This phantom was designed to have acoustic properties similar to tissue (attenuation, speed of sound, thermal conductivity, etc.), the ability to dilute microbubbles without damage, and allow for the visualization of lesion creation. With the help members of the Averkiou lab, needs and design criterion lists were developed.

Table 1. Phantom Needs List

#	Need	Justification
1	Acoustically like human tissue	The Averkiou lab has access to *ex-vivo* pig livers for the next step of these experiments. Ideally, the phantom would mimic liver such that the parameters determined by the *in-vitro* experiments can guide the *ex-vivo* experiments. However, since the medical motivation is for brain treatments, general human tissue similarity is the labeled need.
2	Ability to introduce heterogeneities	The model should allow for microbubble dilution. Also, it should potentially allow for modification to make it more like real tissue, including vessels, walls, and other tissue heterogeneities.
3	Easy to visualize lesion formation & temperature changes	The Averkiou lab does not have access to an MRI to easily visualize temperature changes and lesion formation, so the phantom should allow for easy visualization of lesion formation and allow for temperature measurements (i.e. thermocouple introduction).
4	Thermal properties like human tissue	The phantom should produce a thermal lesion at the same temperature as average human tissue.

Table 2. Phantom Criterion List

Which Need it Addresses	Criterion	Quantitative/Qualitative Value
1	Density (avg. human tissue)	1.076 g/mL [35],[36]
1	Attenuation Coefficient (avg. human tissue)	0.58.5 ± 0.35 dB/cm/MHz [38],[39]
1	Speed of Sound (avg. human tissue)	1565.5 m/s [37]
2	Moldable Model	Liquid → Solid State
3	Optical Transparency	See-through
4	Temperature Denaturation	60 °C [32]

To visualize phantom burning during and after ultrasound treatment, the phantom should, ideally, be optically transparent and undergo a temperature dependent color change. It is important that the phantom accurately represents the coagulation temperature of human tissue. Full burns occur in the skin at 60°C within 6 seconds (Figure 3). As the ratio of blood to tissue increases, thermal sensitivity decreases and the temperature response becomes more complex, due in part to water's high specific heat capacity [32]. Generally, complete necrosis occurs instantaneously at 60°C for most cell types [31]. As the tissue temperature rises to 60°C, the time required to achieve irreversible cell damage decreases exponentially. An area of coagulative necrosis develops in the liver at temperatures between 60 and 140 C [33].

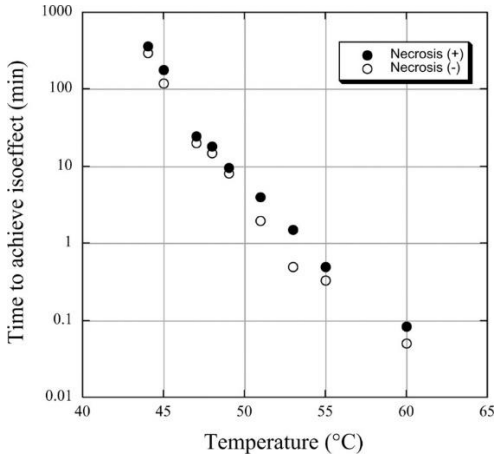

Figure 3: This picture depicts the thresholds for thermal damage for skin. The open circles indicate the highest time-temperature combination studied for which there was no burn and the solid circles indicate the lowest combination that caused a burn [32].

An experimental setup was designed to perform the BEH experiments. This required a method by which to implement real-time ultrasound image guidance and to measure real-time temperature measurements at the focus. Once an experimental setup and protocol was created, the parametric study was designed. To determine microbubble concentration effect on heating, three different concentrations were picked based on the clinical range for imaging and preliminary experiments (EXP)completed in the Averkiou lab (1e2, 1e3, 1e4 MB/mL). To study the effect of pressure on microbubble-induced heating, three different pressures were chosen based on preliminary experiments (0.5, 2, 6 MPa). The research plan in Table 3 was followed:

Table 3. Parametric Study Experiment List

pressure / concentration	0.5 MPa	2 MPa	6MPa
No MBs	EXP 1	EXP 2	EXP 3
1e2 MB/mL	EXP 4	EXP 5	EXP 6
1e3 MB/mL	EXP 7	EXP 8	EXP 9
1e4 MB/mL	EXP 10	EXP 11	EXP 12

2. Materials

The various iterations of the tissue-mimicking phantom required the following materials: Polyvinyl Alcohol, Dimethyl sulfoxide (DMSO) solvent, Cellulose, 40% Acrylamide solution, Egg-white, 10% Ammonium Persulfate, Tetramethyl ethylenediamine (TEMED), Glycerol, Tris buffer, and Bovine Serum Albumin. To create the phantoms, a source of DI water, a mixing plate, (4) 250 mL beakers, an automatic pipette, PPE, a refrigerator, (2) 150 mL plastic boxes, (16) 75 mL plastic boxes, and a fume head were required. Diluting microbubbles into the phantom required the following four microbubbles: an in-house Definity-like microbubble, Optison (human albumin microspheres; GE healthcare AS; Mallinckrodt Inc., San Diego, CA) microbubbles, SonoVue (Sulfur Hexafluoride microbubbles; Bracco Imaging SpA, Colleretto Giacosa, Italy; also marketed as Lumason in the USA) microbubbles, and Sonazoid (Perfluorobutane; Daiichi Sankyo Co. Ltd., Tokyo, Japan) microbubbles. The in-house Definity-like microbubbles, composed of DPPC (1,2-dipalmitoyl-sn-glycero-3-phosphocholine) and DSPE-PEG (1,2-distearoyl-sn-glycero-3-phosphoethanolamineN-[methoxy(polyethylene glycol)-2000]) (Avanti Polar Lipids Inc, Alabaster, AL) in a 95:5 molar ratio, were prepared as previously described in (Cock et al., 2015; Temmerman et al., 011).

To measure the temperature, multiple thermocouples were tested: a 40-gauge thermocouple (5TC-TT-T-40-72, Omega Engineering Inc., Norwalk, CT, USA), a 33-gauge thermocouple (HYPO-33-1-K-60-SMPW-M, Omega Engineering Inc., Norwalk, CT, USA), and a 26-gauge thermocouple (MT-26/2HT Needle Microprobe, Physitemp Instruments Inc., Clifton, NJ, USA). The thermocouples were attached to a National Instruments USB Data Acquisition Device (cDAQ-9171 NI 9212; National Instruments, Austin, TX, USA).

The final experimental setup were performed in a water tank and used the Philips iU22 ultrasound imaging system (transducer: L9-3; Philips, Bothell, WA, USA) as the real-time imaging component, a focused single element circular transducer (diameter = 64.0 mm, focal distance = 63.2 mm, frequency = 0.9 MHz) (H-116, Sonic Concepts, Seattle, WA, USA) as the HIFU transducer, and two mechanical positioners, one for each transducer. To align the setup, the HIFU transducer was connected to a motion controller, which was controlled using a custom LabVIEW VI (National Instruments, Austin, TX, USA) and pulse-echo measurements were taken using an oscilloscope controlled by a separate custom LabVIEW VI. The characterization of the HIFU transducer can be seen in Figure 4. This Figure shows two experimental measurements from a beam pattern taken at the focus and a propagation curve along the axis of the transducer. The measured focal area was 2.5 mm wide and 15.4 mm long. The 2D normalized pressure field was computed using the Rayleigh integral using MATLAB to verify the results. The data was processed using MATLAB (MathWorks) and QLAB (Philips Healthcare).

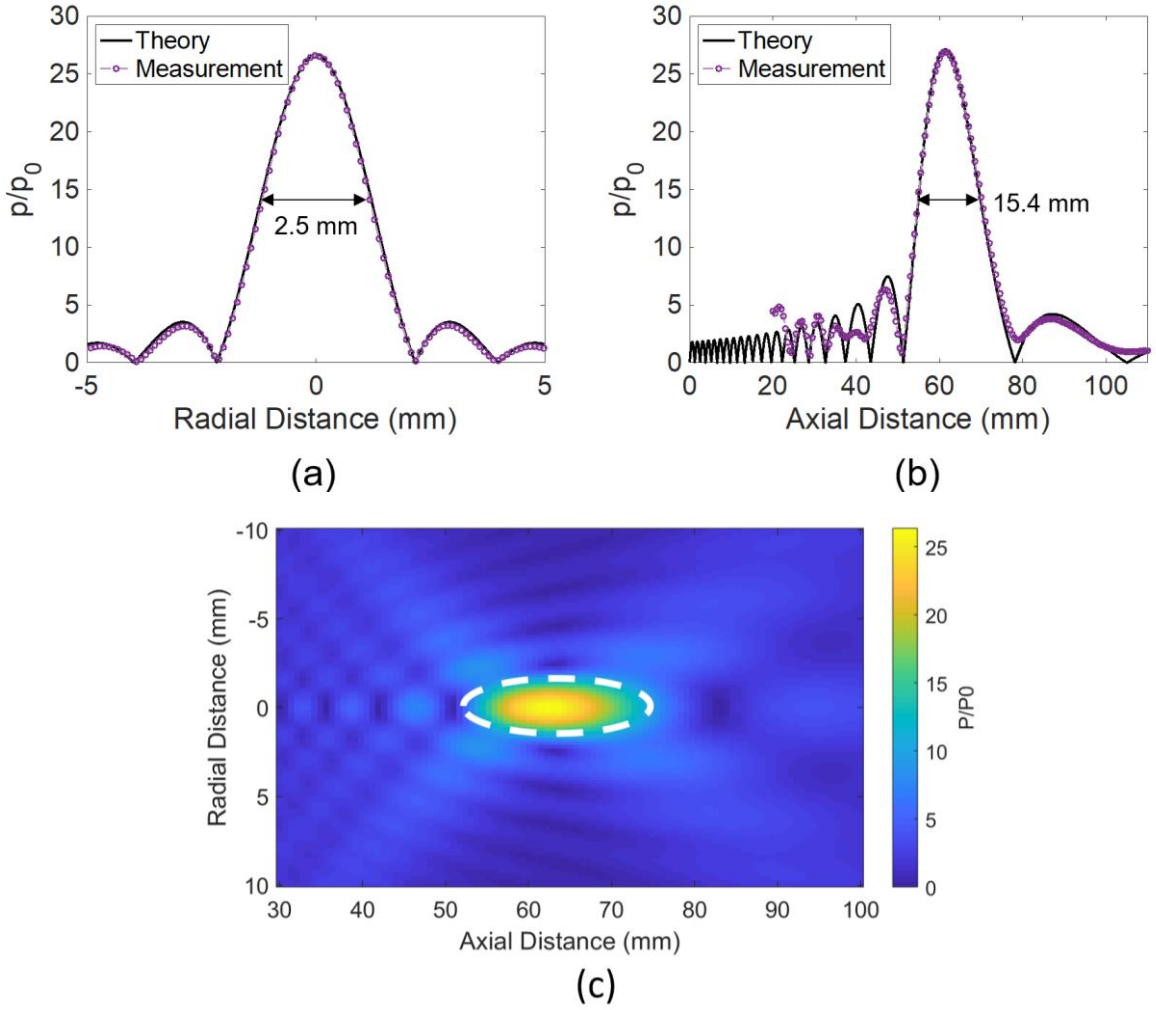

Figure 4: Measurements were taken of the HIFU transducer in degassed and deionized water to verify the area of the focus. (a) Beam pattern taken at the focus of the transducer (2.5 mm). (b) Propagation curve taken along the axis of the transducer (15.4 mm). (c) The 2D normalized pressure field computed using the Rayleigh Integral with the focal area circled.

3. Methods: Development of the In-Vitro Research Platform

3.1 Phantom Characterization

To visualize and measure the therapeutic effect of BEH, three optically transparent phantoms were chosen from the literature: a Polyvinyl Alcohol-based (PVA) gel, and two Acrylamide-based gel. The two Acrylamide-based gel variations contain different animal proteins (Bovine Serum Albumin (BSA) and Egg-white) used as temperature indicators. The phantoms were compared using the following parameters: density, attenuation, speed of sound, budget, and optical transparency. The density was measured by taking the weight of the phantom and dividing it by the volume it displaces in water. The attenuation was measured by placing the phantom into a water bath on top of an absorbing pad and using the Philips iU22 system and the L9-3 probe with a specified imaging setting, we took an

image. Then, we removed the phantom and took the same image with the same imaging settings. Using QLAB, we drew a region of interest around the absorbing material boundary and recorded the Decibels (dB) for both the images with phantoms and those without the phantoms. Comparing the two dBs, we determined the ΔdB (dB without phantom – dB with phantom). Using the following equation with a known width of phantom and known frequency, we calculated the attenuation:

$$Attenuation = \frac{dB}{cm * MHz}$$

The speed of sound was measured using the images from the attenuation measurements by measuring the distance from the top of the phantom to the bottom of the phantom. The Philips iU22 assumes a speed of sound of 1540 m/s. By using this assumption, we can find the phantom speed of sound with the following expression:

$$\frac{d(actual)}{d(image)} = \frac{c(actual)}{\frac{1540m}{s}}$$

The three phantoms were compared by budget by calculating the cost for an 100mL phantom. Table 4 compiles all the results. Based on similar human tissue properties and the lowest cost, the egg-white phantom was chosen.

Table 4. Phantom Comparison

parameter / phantom	Density (kg/m^3)	Attenuation (dB/cm/MHz)	Speed of Sound (m/s)	Cost ($/100mL)	Transparent (Y/N)
PVA	1000	0.38	1600	~13	Y
BSA	1020	0.11	1501	~14	Y
Egg-White	1058	0.25	1546	~8	Y*

Y*: The phantom's transparency depended on the transparency of the batch of egg-white purchased from the store. Some batches would be transparent and then others wouldn't.

Once the various phantom type's acoustic properties were tested and the egg-white phantom chosen, tests were performed to check that the phantom met need #4, thermal properties similar to human tissue. To test this, an egg-white phantom was prepared. The egg-white phantom was prepared following a recipe developed by Takegami et al. (2004) [13]. All the materials (for materials refer to table 10) are combined except for Ammonium Persulfate and TEMED (cross-linkers). To remove extraneous gas, the solution is placed into a vacuum to degas. The solution is liquid until the cross-linkers are added. The two undergo an exothermic reaction, solidifying the solution into the gel. While the solution is solidifying, it is placed in the fridge to decrease the max temperature of the solution. This became the standard protocol followed for the creation of egg-white phantoms for future BEH experiments.

Once the phantom solidified, it was removed from the fridge to return to room temperature. The phantom was cut into 1.88 cm x 1.88 cm x 1.67 cm pieces. A water bath was warmed to five target temperatures (50, 55, 60, 65, & 70 °C) and a stand was placed in the water bath so the phantom was suspended above a hotplate (see Figure 5 for setup). The phantom never came in direct contact with the hotplate and a stir bar was placed below to circulate the temperature to avoid hot and cold regions. Two thermocouples were used: one was placed in the center of the phantom piece (TC1) and the other was placed in the water bath near the phantom (TC2).

Each trial used the following procedure:

1) Wait until water reaches target temperature (seen by T2)
2) Put phantom in the water
3) Wait until T1 reaches T2
4) Pull phantom out of water
5) Image phantom piece next to untreated phantom

Table 5 is a reference for phantom number and temperature experiments. It includes the time it took for the center of the phantom to reach the target temperature, the temperature in the water bath (time till TC1 reached TC2). Figure 6 shows the images of each phantom piece after the time spent in water bath. The untreated phantom, the phantom treated with 50 °C, and the phantom treated with 55 °C were optically transparent after being treated, and the phantom treated at 60 °C was cloudy. This indicated that the phantom treated at 60°C had irreversible damage.

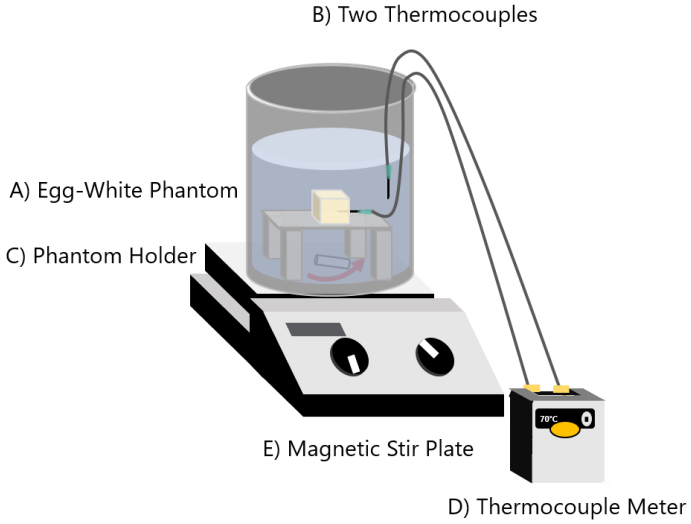

Figure 5: To study the egg-white phantom denaturation temperature, this experimental protocol was used. The egg-white phantom (A) was placed on a holder (C) inside a beaker on a magnetic stir plate (E). Two thermocouples (B) were placed in the ambient water and inside the phantom and a thermocouple meter (D) measured the temperature.

Table 6. Phantom Identification and Summary

Phantom #	Start temperature of water bath **T2** (℃)	Time till target temperature reached (s)	Noticeable discoloring (Y/N)
1	50	329	**N**
2	55	379	**N**
3	60	388	**Y**
4	65	434	**Y**
5	70	655	**Y**

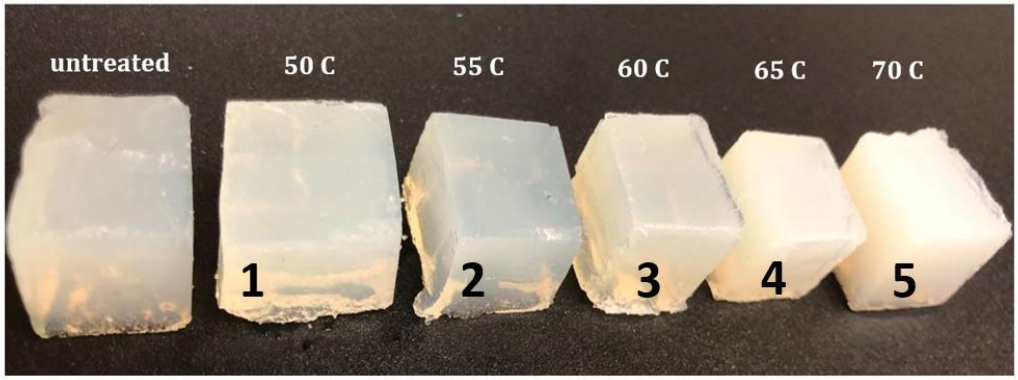

Figure 6: The phantoms after treatment are seen. The untreated phantom, phantom 1 (50℃), and phantom 2 (55℃) are optically transparent. Phantom 3 (60℃), 4 (65℃), and 5 (70℃) are cloudy.

Through the phantom creation process, the crosslinking material (Ammonium Persulfate and TEMED) undergo an exothermic reaction that solidifies the gel. The solution changes state from a liquid into a solid in a rapid manner. To dilute microbubbles throughout the solution, the microbubbles needed to be introduced before the crosslinking material. To check that microbubbles could withstand the reaction, temperature measurements were taken. Microbubbles are stored in a refrigerator and then are used for ultrasound contrast imaging, so they should be stable between 4-40 °C.

11 phantoms were created using the standard protocol. Three of which had 80% of the concentration of crosslinkers (shown in table 10), four had the normal concentration of crosslinkers, and four had 120% of the concentration of crosslinkers. Multiple concentrations of crosslinkers were tested to see if changing the concentration effected heat of reaction. Once the solutions were mixed, a thermocouple was placed in the solution. The solution, thermocouple, and thermocouple meter were placed in the fridge and allowed to solidify over the course of 45 minutes. Figure 7 shows the plots of the temperature of reaction for each of the concentrations. The highest temperature rise occurred in the phantoms with 120% of the concentration of crosslinkers. All the plots were zeroed to get the change in temperature, instead of the absolute value. However, all

experiments started at room temperature, 21 °C. The absolute max for 80% was 36°C, for 100% was 38°C, and for 120% was 42°C. Since the temperature throughout the reaction for the regular concentration of crosslinkers remained inside microbubble stability range, 100% concentration of crosslinkers was used as the preferred concentration, as described in table 10.

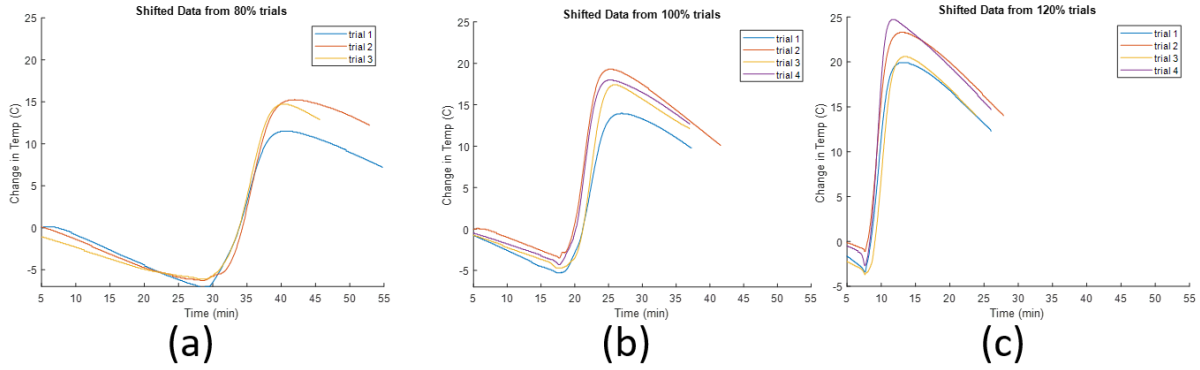

Figure 7: Measurements were taken of the heat of reaction in phantoms with 80%, 100%, and 120% of crosslinkers. (a) 80% of the crosslinkers temperature change over time plot can be seen. It had the lowest temperature rise. (b) 100% of crosslinkers temperature change over time plot can be seen. (c) 120% of crosslinkers temperature change over time plot has the highest temperature rise and over the shortest time.

3.2 Microbubble Dilution

The Averkiou lab has access to multiple types of microbubbles: Definity-like, Optison, Sonovue, and Sonazoid microbubbles. The standard protocol to make egg-white phantoms was tested using the four different microbubbles. The solution was prepared and prior to introduction of crosslinkers, 10^4 MB/mL was mixed into the solution. The liquid phantom solution was imaged using the Philips iU22 ultrasound system and an L9-3 transducer using contrast imaging prior to the addition of cross-linkers. Then, the cross-linkers were added, and the solution was left to polymerize in the refrigerator. Once the phantom was fully solidified, the phantom was imaged using the same ultrasound parameters. Using contrast imaging to monitor for the presence of MBs, the multiple types of manufactured MBs were tested and we found that some would show up in the phantom and some would not. Figure 8 shows an example of the contrast images of Definity-like, Optison, Sonovue, and Sonazoid in the phantom solution pre-polymerization side-by-side with the contrast images of the same phantom post-polymerization. Definity-like, Optison, and Sonovue didn't show up in the phantom in these example Figures. Table 7 summarizes the experiments performed with the four different microbubbles. Sonovue showed up half of the time, Optison never showed up, Definity-like bubbles were not consistent, and Sonazoid always showed up.

Sonazoid showed up, but there was an obvious decrease in image intensity. To determine the approximate loss of bubbles through the polymerization process, the

phantom with Sonazoid was analyzed in QLAB before and after the crosslinkers were added. Two regions of interest (ROI) were drawn such that the entire illuminated volume was analyzed and a small subsection in the middle of the volume was analyzed. The ROI's can be seen in Figure 9. QLAB analyzed the average intensity over the two ROI's at each time point in the ultrasound loop. The output results from the QLAB analysis were plotted in excel and can be seen in Figure 10. It was determined that Sonazoid was the most stable and reliable bubble, so it was used for all BEH experiments.

Table 7. Microbubble Dilution Experiment Summary

Type	Present Post-Polymerization	# of Trial
Definitely-like	Not consistent	>5
Optison	Never showed up	>5
Sonovue	Showed up half the time	>5
Sonazoid	Always showed up	3

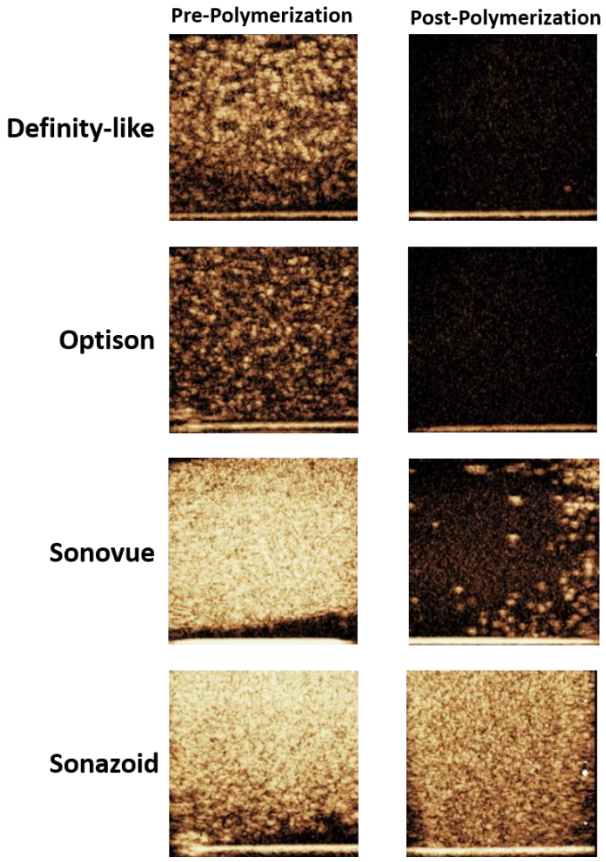

Figure 8: These images are nonlinear contrast-enhanced ultrasound images (AM) that detect microbubbles. The Definity-like, Optison, and Sonovue microbubbles don't show up in the phantoms post-polymerization, while Sonazoid does.

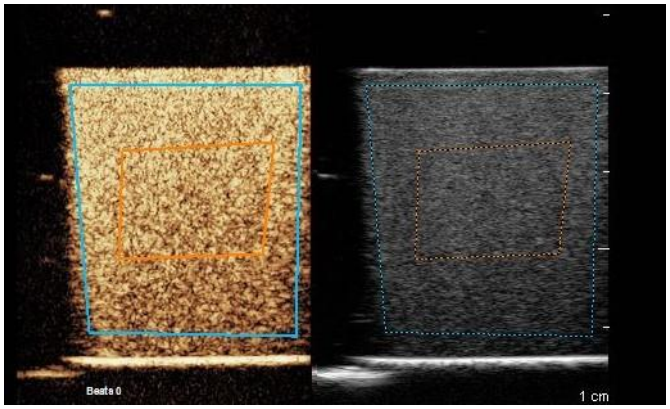

Figure 9: This Figure depicts the ROIs (ROI #1 – large; ROI #2 – small) chosen for QLAB analysis. This is an image of a solution with Sonazoid bubbles without crosslinkers.

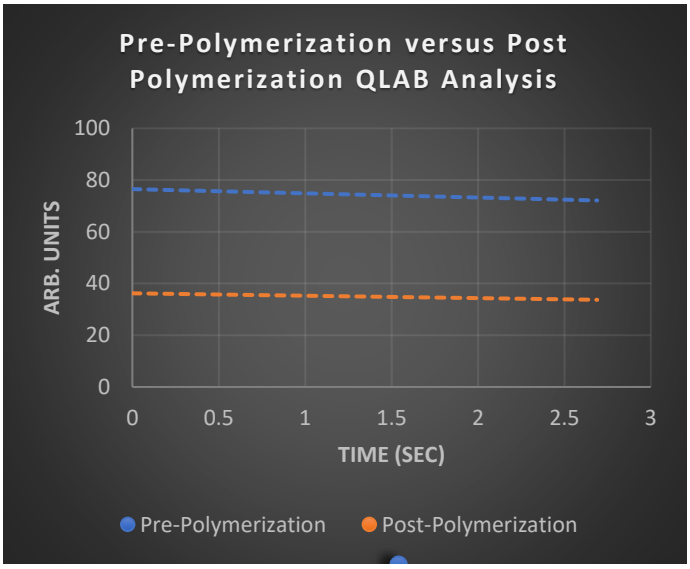

Figure 10: This plot is the output from the QLAB analysis. The mean of the intensity is plotted along the y-axis and the absolute time in seconds along the x-axis. The pre-polymerization has a higher intensity than post-polymerization.

3.3 Temperature Measurement Method

Originally, we had a 40-gage thermocouple in the lab to perform initial preliminary experiments. Our temperature results seemed to be too large and weren't consistent across experiments. After a literature review, we noticed that thermocouples have a known artifact when introduced to a pressure field. A thermocouple is known to absorb some of the acoustic energy and produce heat itself. Because of this, we ordered two other types of thermocouples. To test the three thermocouples, the thermocouples were inserted into egg-white phantoms by hand. Then, the focus of the HIFU transducer was aligned to the tip of the thermocouple using pulse-echo measurements taken by an oscilloscope, controlled by a custom LabVIEW VI. The measurements are taken in a 2D grid pattern in the x and y axes, called a 2-D Beam Pattern (2DBP); the axes can be seen in Figure 11. Then, the results

are plotted using MATLAB seen in Figure 6. Once perfectly aligned, the HIFU transducer was turned on for exactly 30 seconds CW using 0.5 and 1 MPa. This protocol was completed for the three thermocouples. Table 8 is a reference table for thermocouple type.

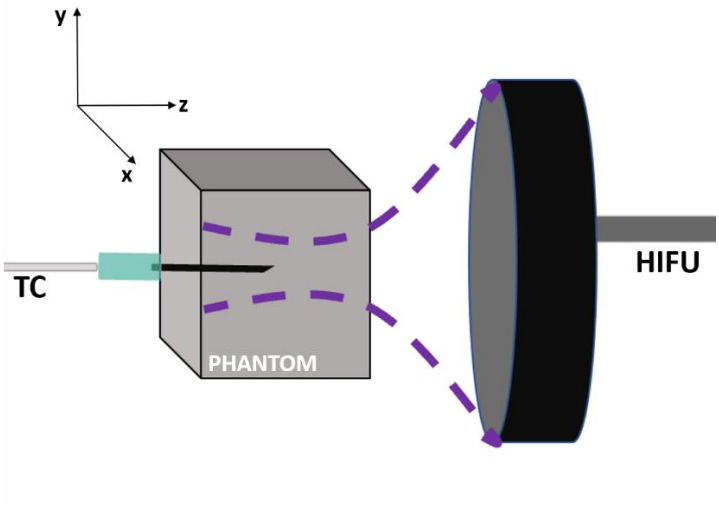

Figure 11: Thermocouples were tested with the above experimental setup. The HIFU transducer is connected to a function generator. The thermocouple is connected to a DAQ. The axes can be seen in the upper right corner of the Figure.

Table 8. Thermocouple Reference

Reference	Name	Gage (AWG)	Diameter (mm)
TC1	5TC-TT-T-40-72	40	0.07874
TC2	HYPO-33-1-K-60-SMPW-M	33	0.18034
TC3	MT-26/2HT Needle Microprobe	26	0.40386

Because of the different sizes and compositions of the three thermocouples, the alignment procedure was easier for two (TC1 & TC3) and difficult for one (TC2). The MATLAB plots for each of the alignment procedures can be seen in Figure 12. For TC2, we aligned using temperature measurements, instead of pulse-echo. We moved the transducer step by step in the x and y axes, turned the HIFU transducer, and recorded the temperature. We found the thermocouple tip by focusing to where temperature was highest. Aligning using pulse-echo uses approximately 45 minutes, while aligning using temperature readings uses ~2 hours.

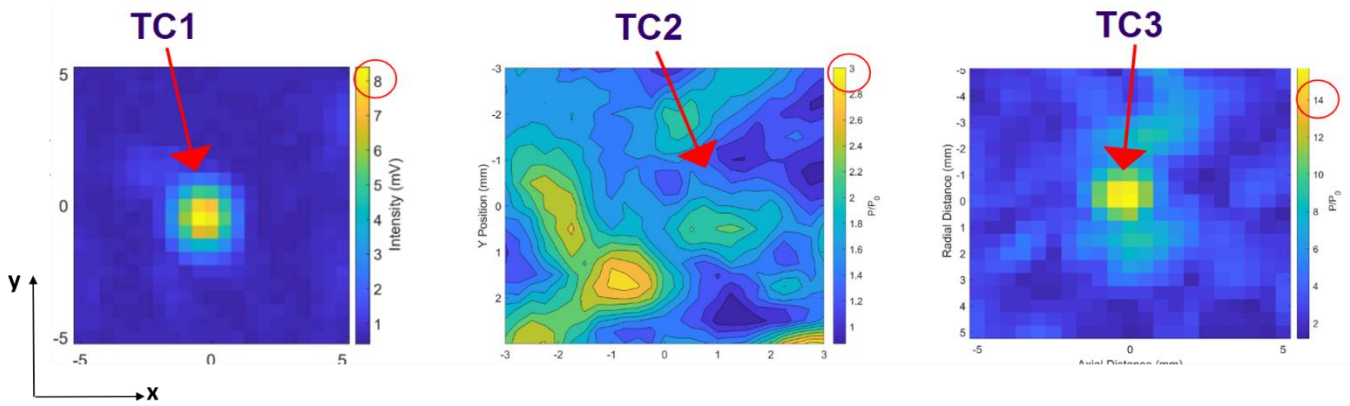

Figure 12: The three pulse-echo alignment results are plotted above. For TC1 and TC3, an obvious peak intensity zone can be seen. For both TC1 and TC3, the normalized pressure at the peak intensity zone are much higher than that seen for TC2 alignment. This alignment procedure didn't work because an obvious thermocouple signal was not received.

Using the theory MATLAB code created by Conner Pitts, the three thermocouples were compared at 0.5 MPa seen in Figure 13. TC1 seemed to overpredict the theoretical temperature and the other two thermocouples were within 0.3 °C of theory. Both TC2 and TC3 seemed to predict the temperature closest to theory with a reasonable error. Since TC3 was the easiest to align to using pulse-echo alignment, we decided to move forward with TC3 with future BEH experiments. This thermocouple is a needle microprobe and is known to reduce the effect on the acoustic field.

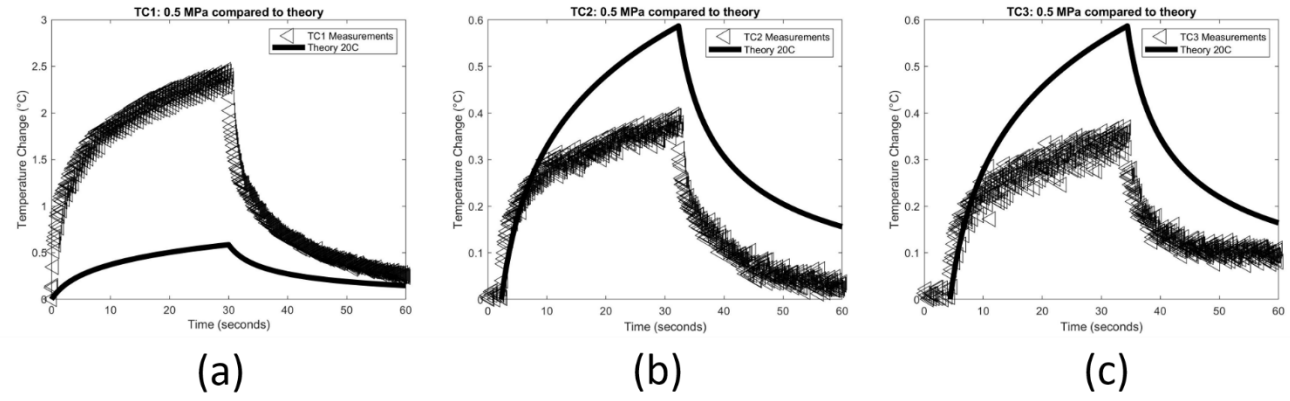

Figure 13: Measurements for thermocouple HIFU-induced temperature rise are plotted. (a) TC1 was plotted against theory at room temperature. The thermocouple measurements overpredicted what theory states. (b) TC2 was plotted against theory at room temperature and was lower than theory by 0.25 °C. (c) TC3 was plotted against theory at room temperature and was lower than theory by 0.3 °C.

Results

1. Final *In-Vitro* Research Platform Design & Experimental Protocols

The finalized egg-white phantom properties are described in table 9 and the materials and percent makeup are described in table 10. The finalized concentration of microbubbles diluted throughout the phantoms can be seen in Figure 14.

Table 9. Overview of Egg-white Acoustic Properties

Density (kg/m^3)	Speed of Sound (m/s)	Attenuation. (dB/cm/MHz)	Thermal Conductivity (W/m/K)	Specific Heat Capacity (kJ/kg/K)
1.058	1545.67	0.25 ± 0.05	0.59±0.06	4.27±0.37

Table 10. Materials and Percent Makeup

material	percent (%)
40% Acrylamide Solution	24.8
Degassed Water	40
Egg White	30
10% Ammonium Persulfate	0.5
TEMED	0.2
Glycerol	4.5

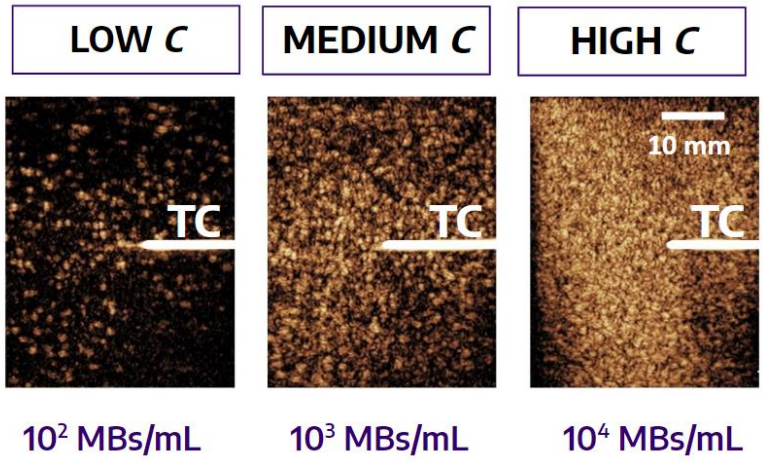

Figure 14: 10^2, 10^3, and 10^4 MB/mL (low, medium, and high) were chosen based on the microbubble clinical concentration range for imaging. These images are nonlinear contrast-enhanced ultrasound images (AM) that detect microbubbles. These images are taken post-polymerization and with the thermocouple inserted into the phantom (TC).

To maintain consistency, a setup and alignment procedure was created to align the HIFU transducer to the thermocouple tip inside the phantom and align the imaging probe to the thermocouple in the transverse plane. The procedure was as follows:

1. The phantom was placed inside the water tank in front of the HIFU transducer and then the imaging probe was aligned to the thermocouple using the motion controller. Figure 15 explains the setup step-by-step. The finalized experimental setup can be seen in Figure 16.

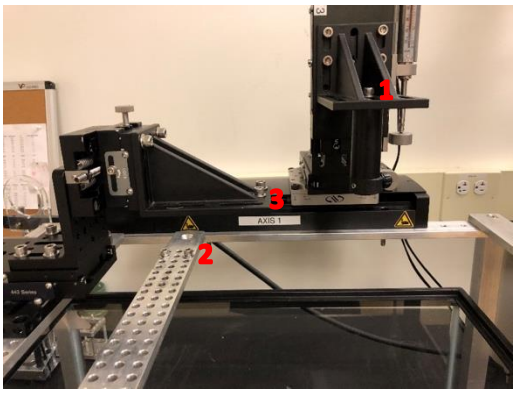

Figure 15: This Figure depicts the two motion controllers. The HIFU transducer was placed in the adjustable attachment at location 1. Then, the phantom holder with the phantom was secured at location 2. Then, the imaging transducer was attached to location 3.

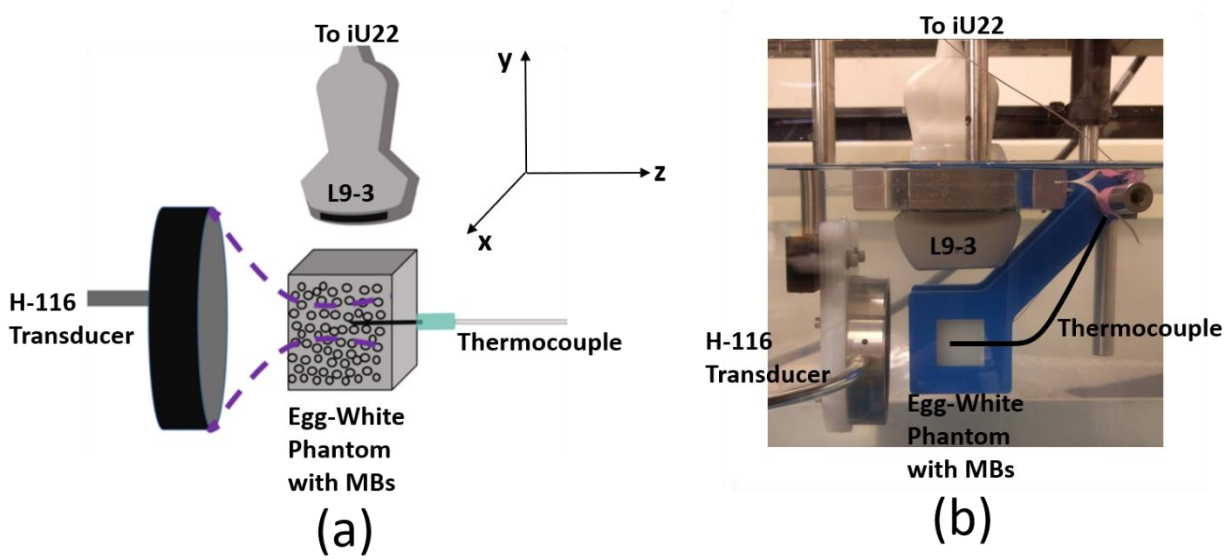

Figure 16: This Figure is the finalize experimental setup. (a) Schematic of the H-116 transducer with the inserted thermocouple. The thermocouple tip is aligned to the focus of the H-116 transducer. The imaging plane of the L9-3 imaging array is aligned perpendicular to the H-116 axis of propagation. (b) Photograph of the experimental setup.

2. Using pulse-echo signals on the oscilloscope, the front wall of the phantom was found by moving the HIFU transducer in the z-axis using an automatic motion controller. There was a large signal on the oscilloscope at the focus of the transducer, corresponding to the following time.

$$t = 2\left(\frac{d}{c}\right)$$

Where t is the time on the oscilloscope, d is the transducer focus, and c is the sound speed.

3. Using the Philips iU22 ultrasound system, the approximate distance from the front of the phantom to the thermocouple tip was measured using the calipers.
4. Using a custom LabVIEW VI, the HIFU transducer was moved to the measured location on the motion controller (ex. Motion Controller Value = Focus - Distance Measured; in the z-axis).
5. Using the automatic motion controller, the HIFU transducer was moved in axis 2 (x axis) and axis 3 (y axis) to where there was a maximum signal on the oscilloscope.
6. Once the approximate center was estimated, a 2D Beam Pattern (2DBP) was taken using a custom LabVIEW VI. Using this 2DBP, the HIFU transducer was moved to the tip of the thermocouple. Figure 17 shows an example of this.

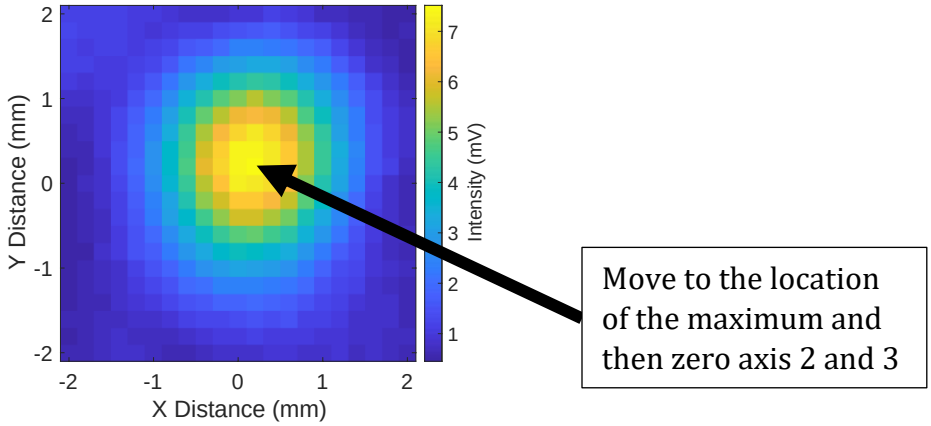

Figure 17: MATLAB plot using the data from the 2D Beam Pattern taken using the custom LabVIEW VI. The highest intensity value can be seen at the tip of the black arrow. This is where the tip of the thermocouple is located.

Once the HIFU transducer was aligned using the alignment procedure, the egg-white phantom was treated with the HIFU transducer for 30 seconds at an 82% duty cycle (on for 370,000 cycles). The ultrasound images were interleaved with the treatment, so there weren't any artifacts in the real-time image guidance. The imaging was used to monitor the behavior of the microbubbles throughout treatment and to image lesion formation. Interleaved ultrasound images were taken for the 30 seconds during treatment and then

for another 30 seconds after the HIFU transducer was turned off. The temperature was recorded by the thermocouple for the 30 seconds during treatment time and for 30 seconds after. Figure 18 depicts a schematic of the pulsing sequence with real-time image guidance.

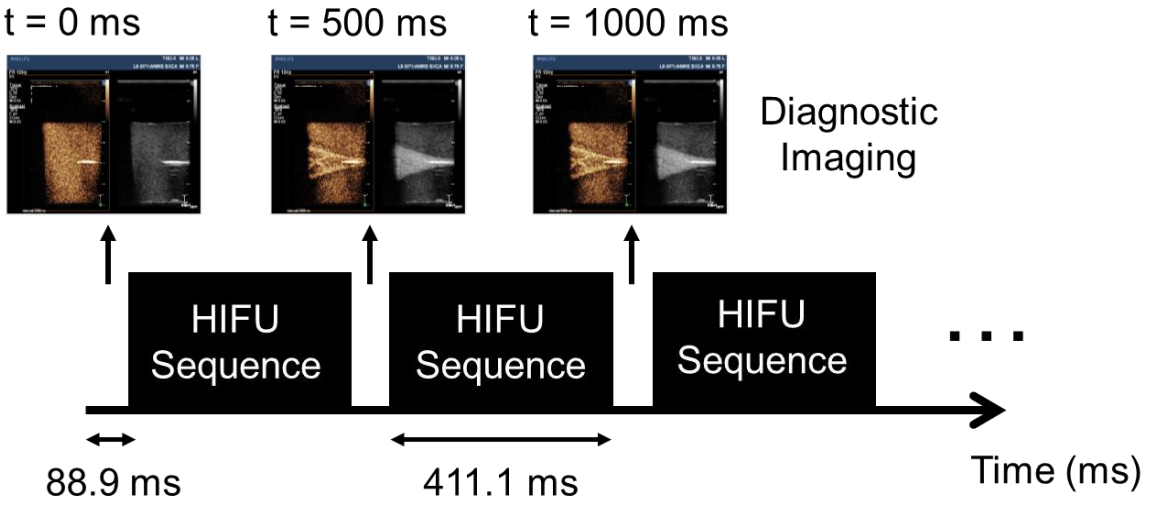

Figure 18: Schematic of the HIFU pulsing sequence with interleaved diagnostic imaging (L9-3 probe). The HIFU transducer was turned on for 411.1 ms and then off for 88.9 ms and during this time a diagnostic ultrasound image was taken. This was repeated for the entire treatment time (30 s).

2. Temperature & Imaging Results

The experiments from table 3 were performed using the finalized *in-vitro* research platform and protocol from the previous section. Figure 19 shows the temperature measurements from the three different pressure amplitudes (0.5, 2, and 6.0 MPa). At the lowest pressure (0.5 MPa), there was an error in the measurement for the lowest concentration (1e2 MB/mL) and this experiment would have been repeated given more time for experiments. However, the other two microbubble concentrations (1e3 and 1e4 MB/mL) increase the temperature rise in comparison to the phantom without microbubbles. At 2.0 MPa, the same trend is seen: the presence of microbubbles increases the temperature rise, except for the highest concentration (1e4 MB/mL). The highest pressure (6.0 MPa), only the lowest concentration (1e2 MB/mL) increases the temperature rise at the thermocouple in comparison to the phantom without microbubbles. As seen in Figure 20, the highest concentration consistently saw less than a 5°C increase in temperature at the thermocouple across all pressures. Since this wasn't what we had hypothesized occurring, we performed the experiment again and inserted a thermocouple at the face of the phantom. Figure 21 shows the results from both a focal thermocouple and a front face thermocouple the highest concentration (1e4 MB/mL) and highest pressure (6.0 MPa). Temperature at the front of the phantom showed >40°C greater temperature rise than the focal thermocouple.

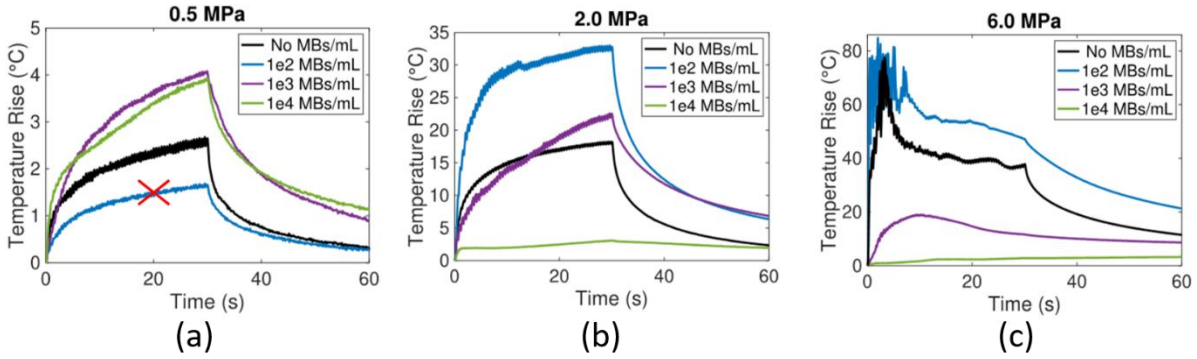

Figure 19: Temperature measurements from the HIFU experiments. (a) 0.5 MPa experiments. The highest two concentrations have a higher temperature rise compared to the phantom without microbubbles. The lowest concentration (1e2 MB/mL) was incorrectly aligned to in the experiment. (b) 2.0 MPa experiments. The low and medium concentrations saw increased temperature rise. (c) 6.0 MPa experiments. Only the lowest concentration saw increased temperature rise.

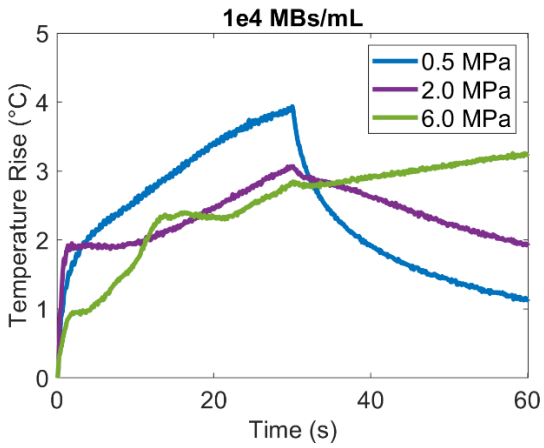

Figure 20: The three pressure amplitudes for the highest concentration plotted together. None of the temperature rises increased past 5°C at the thermocouple tip.

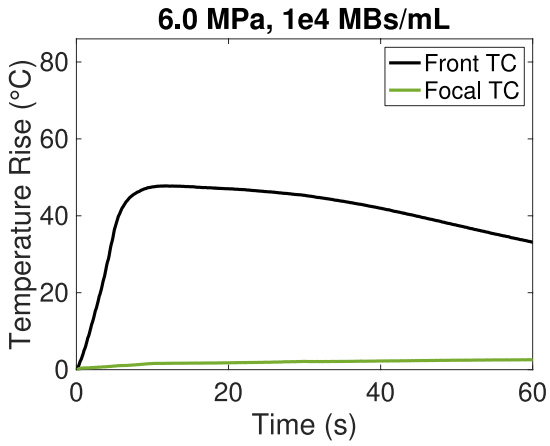

Figure 21: Two thermocouple readings from a HIFU treatment at 6.0 MPa with the highest microbubble concentration. The front thermocouple saw >40°C temperature compared to the focal thermocouple.

To better understand microbubble activity, we analyzed the ultrasound images. Figure 22 shows the ultrasound images after the first HIFU sequence (370k pulses) for the three concentrations at the medium pressure (2.0 MPa) and the H-116 2D normalized beam pattern with the expected beam path outlined for reference. The therapeutic ultrasound propagates from left to right and the focus of the transducer is aligned to the tip of thermocouple seen as a white bar in the Figures. The images were taken using conventional fundamental ultrasound imaging. The beam path was outlined in each of the images for easy visualization. At the lowest concentration (1e2 MB/mL), the expected beam pattern can be seen. However, at the medium and high microbubble concentrations,

the bubble activity isn't symmetric. This signifies that the sound field throughout the phantoms with higher concentrations isn't symmetric. Thus, the microbubbles are distorting the sound field and attenuating the sound from penetrating through the entire phantom.

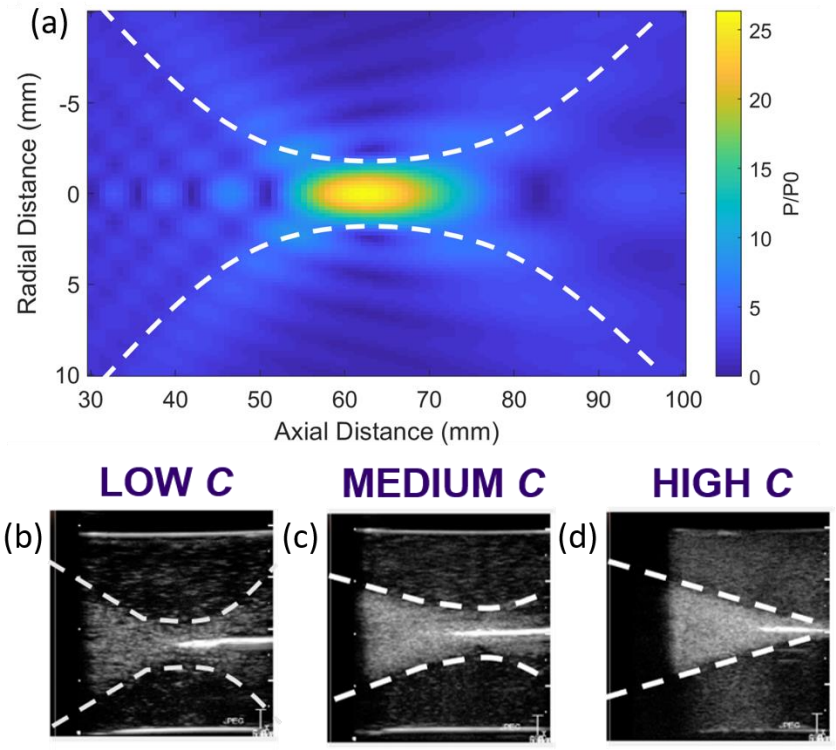

Figure 22: Fundamental images after the first HIFU sequence (370k pulses). (a) H-116 2D normalized beam pattern MATLAB plot using the Rayleigh integral with the beam path outlined for reference. (b)The symmetric beam pattern can be seen at the lowest concentration. (c) The slightly asymmetric beam pattern can be visualized at the medium concentration. (d) A triangular shape pattern can be seen at the highest concentration.

Figure 23 shows images of the lesions in three phantoms at 6 MPa and the H-116 2D normalized pressure field with the highest-pressure focal zone outlined for reference. At the lowest microbubble concentration (1e2 MB/mL), the lesion is tadpole-shaped at the thermocouple tip. The X signifies where the thermocouple tip and the HIFU transducer focus were located. As the concentration increases the size and the shape of the lesion changes. At the highest concentration (1e4 MB/mL), the lesion occurs right at the front face of the phantom due to the large amount of attenuation by the microbubbles. The lesions being at the front face makes sense with the front thermocouple experiment performed at 6 MPa.

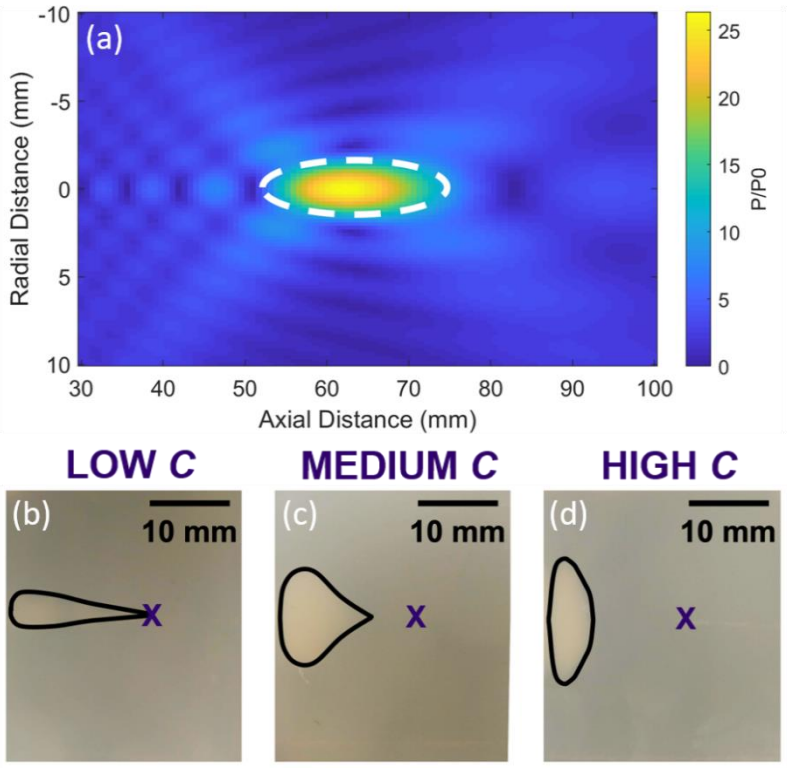

Figure 23: Photographs taken of the phantom post-treatment at 6.0 MPa showing the lesion. (a) H-116 2D normalized beam pattern MATLAB plot using the Rayleigh integral with the highest-pressure focal zone outlined for reference. (b)The symmetric beam pattern can be seen at the lowest concentration. (c) The slightly asymmetric beam pattern can be visualized at the medium concentration. (d) A triangular shape pattern can be seen at the highest concentration.

Discussion

1. Analysis & Conclusions

Thermocouple measurements were taken during the HIFU experiments with three concentrations of microbubbles (1e2, 1e3, 1e4 MB/mL) at three pressures (0.5, 2, 6 MPa). The thermocouple results gave insight into the effect microbubbles have on thermal ablation. Additionally, further temperature analysis gave insight into the relationship between microbubble concentration and spatial temperature mapping. The results help to outline the increase in temperature rise from microbubble activity when there is not excessive attenuation. It is important to note that microbubbles increased the temperature rise even when there was attenuation, but the zone of increased temperature rise was closer to the front face of the phantom. This was seen in the front thermocouple experiment. The temperature measurements also underscore the relationship between microbubbles and pressure. To maintain heating in the focal zone, it is important to keep the microbubble concentration low. As seen in Figure 19, the medium concentration at the lowest pressure raised the temperature rise above the phantom without microbubbles, but at the highest pressure, the temperature rise was below. Even though the microbubble

concentration for both was 1e3 MB/mL, the microbubbles attenuated the field more in the higher-pressure case. Both pressure and concentration play an important role in bubble-enhanced heating.

Additionally, real-time imaging was used to visualize microbubble activity during the HIFU experiment and aided the exploration of microbubble behavior during post-processing. As seen in the ultrasound images in Figure 22, the microbubble concentration effected the sound field and attenuated the sound penetration. Real-time imaging also helped us visualize lesion formation over time. The results from the 6.0 MPa experiments lead us to believe that lesion size, shape, and location is also a function of pressure and concentration. The temperature measurements and real-time image guidance allowed us to study the microbubble effect on the heating of the egg-white phantom throughout the course of treatment. For clinical translation, real-time imaging guidance will be a necessity and the process by which to implement interleaved contrast-enhanced ultrasound imaging was described in this work.

This capstone project developed an *in-vitro* research platform to study microbubble enhanced heating during focused ultrasound treatment with interleaved real-time, contrast-enhanced ultrasound imaging. A set of experiments were performed using the platform and the data was analyzed. Microbubble-enhanced heating was studied using in egg-white phantoms at three microbubble concentrations and three pressure amplitudes. When there was not excessive attenuation, microbubbles increased the temperature in the phantoms compared to phantoms without microbubbles. The pressure versus microbubble concentration relationship was studied and is well understood. Also, real-time imaging guidance was implemented and was instrumental in observing microbubble dynamics throughout treatment.

This project lasted 12 months (see table 11). Phase 1 (design and characterization of an optimal tissue-mimicking phantom) was completed by September 2019 on time. Phase 2 (bubble enhanced study) was completed on time by March 2020. Phase 3 (*ex-vivo* study) was not completed because of COVID-19.

Table 11. Gantt Chart for April 2019-June 2020

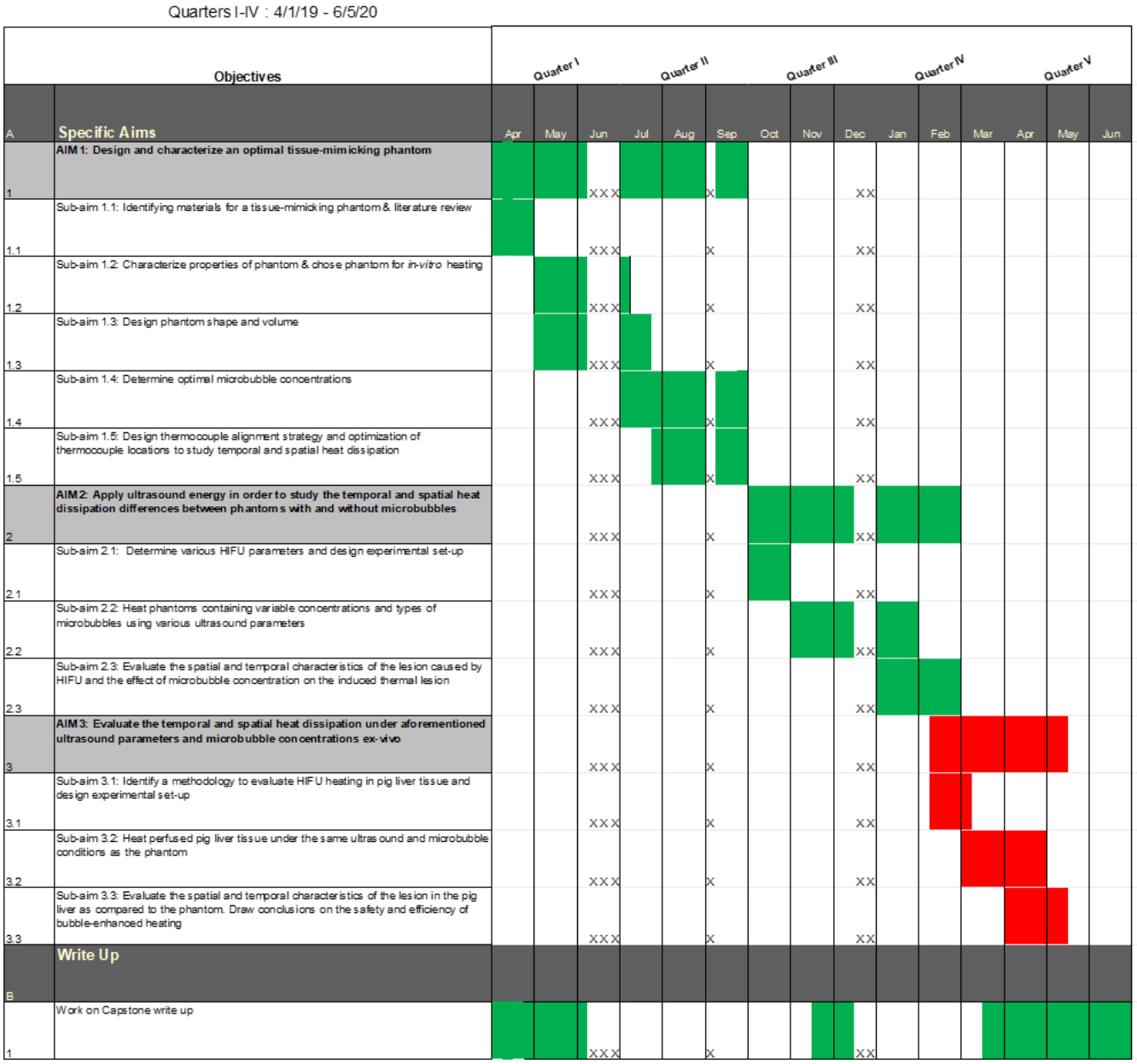

Green = completed, Red = incomplete

2. Future Work

With the *in-vitro* research platform and experimental protocol completed, many other microbubble activity experiments can be performed. Firstly, the experiments studied in this work can be re-done to verify the results and fill in the gaps; for example, the temperature measurement for 0.5 MPa with the lowest pressure should be re-done. Also, clinical microbubbles vary greatly in their chemical makeup. Because of this, different types of microbubbles should be studied to make sure the trend seen in this work is maintained. Also, this work focused on three pressure amplitudes, but a wider range of pressures with a

smaller step size would aid in the development of standardized bubble-enhanced heating protocols. A wider range of pressures would help to determine microbubble and tissue thresholds. Since the medium and high microbubble concentration in this work attenuated the sound field, a set of new concentrations should be studied with the highest concentration being our lowest concentration (1e2 MB/mL).

When microbubbles are introduced clinically, they are injected intravenously and are quickly perfused throughout the vasculature. The microbubbles are approximately the size of red blood cells, so they stay in the blood stream and don't diffuse out into the tissue. In the in-vitro platform, the microbubbles are diluted throughout the phantom with a constant concentration. To address this problem, a proposed experimental setup was designed in Figure 24. This setup would allow for the studying of microbubble activity solely in the focal zone of the transducer. This would reduce the effect of microbubble attenuation and distortion.

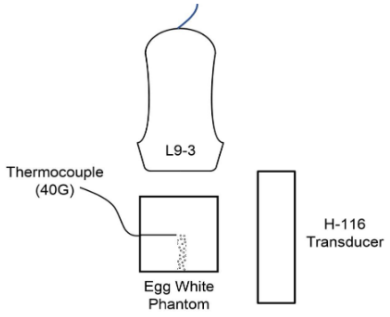

Figure 24: This Figure shows a proposed schematic of the experimental setup with microbubbles inserted locally. It is the same setup as described in Figure 16. This could be used to study microbubbles in the focus and not diluted throughout the phantom.

Ex-vivo pig liver experiments should also be completed with the same three concentrations and three pressures to compare with the trends seen in the *in-vitro* experiments. This could be completed by someone in the Averkiou lab, because the lab has access to *ex-vivo* pig livers. Eventually, human studies will be performed if microbubble-enhanced heating continues to show efficacy through the future experiments.

Acknowledgements

I would like to sincerely thank both Dr. Averkiou and Dr. Clark for their support and direction through my capstone project, and for imparting a love for medical imaging. Dr. Averkiou brought me onto the Averkiou Research Team in the spring of 2018 after a recommendation from Dr. Neils, who I would also like to thank for recognizing my signals and sensors passion and directing me accordingly. I worked under Dr. Dingjie Suo in the Averkiou lab until the spring of 2019. Dr. Averkiou has been instrumental in shaping me as a researcher, communicator, and team member. I also want to thank Dr. Alicia Clark for overseeing and guiding my project from the spring of 2019. Dr. Clark patiently answered all my constant questions regardless of the time or topic. Also, a big thank you to Conner Pitts for his bioheat code that helped guide my experiments and verify my results. I also want to thank Insightech Ltd. For funding the Bubble Enhanced Heating project and Philips for allowing us to use their systems and software.

The Averkiou Research Group comprises of: Dr. Averkiou, Sara Keller, Ting Lai, Eric Juang, Dr. Clark, Pranav Sarda, Kaleb Vuong, Kevin Burgett, Alejandra Cuevas, Katie Thien, Renee Nahum, and Formerly: Sitai Kou, Miguel Monserate, Conner Pitts, Noah Matsuyoshi, Ally Sestero, and Dr. Suo.

Left to right: Sitai Kou, Dr. Suo, Sierra Bonilla, Miguel Monserate, Ally Sestero, Alejandra Cuevas, Conner Pitts, Sara Keller, Noah Matsuyoshi, Dr. Clark, Ting Lai, and Dr. Averkiou.

References

[1] "Cancer," World Health Organization. [Online]. Available: https://www.who.int/news-room/fact-sheets/detail/cancer. [Accessed: 13-May-2019].

[2] "Side Effects of Cancer Treatment | CDC," Centers for Disease Control and Prevention. [Online]. Available: https://www.cdc.gov/cancer/survivors/patients/side-effects-of-treatment.htm. [Accessed: 13-May-2019].

[3] Y.-F. Zhou, "High intensity focused ultrasound in clinical tumor ablation," World journal of clinical oncology, 10-Jan-2011. [Online]. Available: https://www.ncbi.nlm.nih.gov/pmc/articles/PMC3095464/. [Accessed: 13-May-2019].

[4] G. ter Haar, I. Rivens, L. Chen, and S. Riddler, "High intensity focused ultrasound for the treatment of rat tumours," Physics in medicine and biology, Nov-1991. [Online]. Available: https://www.ncbi.nlm.nih.gov/pubmed/1754620. [Accessed: 13-May-2019].

[5] "Essential Tremor," Focused Ultrasound Foundation. [Online]. Available: https://www.fusfoundation.org/diseases-and-conditions/neurological/essential-tremor. [Accessed: 13-May-2019].

[6] Office of the Commissioner, "FDA approves first MRI-guided focused ultrasound device to treat essential tremor," FDA approves first MRI-guided focused ultrasound device to treat essential tremor, 11-Jul-2016. [Online]. Available: https://www.fda.gov/news-events/press-announcements/fda-approves-first-mri-guided-focused-ultrasound-device-treat-essential-tremor. [Accessed: 06-May-2019].

[7] J. Faivre, D. Forman, J. Estève, M. Obradovic, and M. Sant, "Survival of patients with primary liver cancer, pancreatic cancer and biliary tract cancer in Europe. EUROCARE Working Group," European journal of cancer (Oxford, England : 1990), Dec-1998. [Online]. Available: https://www.ncbi.nlm.nih.gov/pubmed/10070285/. [Accessed: 13-May-2019].

[8] T. D. Khokhlova and J. H. Hwang, "HIFU for palliative treatment of pancreatic cancer," Journal of gastrointestinal oncology, Sep-2011. [Online]. Available: https://www.ncbi.nlm.nih.gov/pmc/articles/PMC3397618/. [Accessed: 13-May-2019].

[9] K. S. Bhalsing, J. Saini, and P. K. Pal, "Understanding the pathophysiology of essential tremor through advanced neuroimaging: A review," Journal of the Neurological Sciences, vol. 335, no. 1-2, pp. 9–13, 2013.

[10] N. Chang, S. Lu, D. Qin, T. Xu, M. Han, S. Wang, and M. Wan, "Efficient and controllable thermal ablation induced by short-pulsed HIFU sequence assisted with perfluorohexane nanodroplets," Ultrasonics Sonochemistry, vol. 45, pp. 57–64, 2018.

[11] C. C. Coussios and R. A. Roy, "Applications of Acoustics and Cavitation to Noninvasive Therapy and Drug Delivery," Annual Review of Fluid Mechanics, vol. 40, no. 1, pp. 395–420, 2008.

[12] K. Ferrara, R. Pollard, and M. Borden, "Ultrasound Microbubble Contrast Agents: Fundamentals and Application to Gene and Drug Delivery," Annual Review of Biomedical Engineering, vol. 9, no. 1, pp. 415–447, 2007.

[13] Y. Kaneko, T. Maruyama, K. Takegami, T. Watanabe, H. Mitsui, K. Hanajiri, H. Nagawa, and Y. Matsumoto, "Use of a microbubble agent to increase the effects of high intensity focused ultrasound on liver tissue," European Radiology, vol. 15, no. 7, pp. 1415–1420, 2005.

[14] S. Keller, M. Bruce, and M. A. Averkiou, "Ultrasound Imaging of Microbubble Activity during Sonoporation Pulse Sequences," Ultrasound in Medicine & Biology, vol. 45, no. 3, pp. 833–845, 2019.

[15] V. A. Khokhlova, M. R. Bailey, J. A. Reed, B. W. Cunitz, P. J. Kaczkowski, and L. A. Crum, "Effects of nonlinear propagation, cavitation, and boiling in lesion formation by high intensity focused ultrasound in a gel phantom," The Journal of the Acoustical Society of America, vol. 119, no. 3, pp. 1834–1848, 2006.

[16] O. D. Kripfgans, J. Fowlkes, D. L. Miller, O. Eldevik, and P. L. Carson, "Acoustic droplet vaporization for therapeutic and diagnostic applications," Ultrasound in Medicine & Biology, vol. 26, no. 7, pp. 1177–1189, 2000.

[17] C. Lafon, V. Zderic, M. L. Noble, J. C. Yuen, P. J. Kaczkowski, O. A. Sapozhnikov, F. Chavrier, L. A. Crum, and S. Vaezy, "Gel phantom for use in high-intensity focused ultrasound dosimetry," Ultrasound in Medicine & Biology, vol. 31, no. 10, pp. 1383–1389, 2005.

[18] H. Lea-Banks, M. Oreilly, and K. Hynynen, "Ultrasound-responsive droplets for therapy: A review," Journal of Controlled Release, vol. 293, pp. 144–154, 2019.

[19] M. C. L. Peek, M. Ahmed, A. Napoli, B. T. Haken, S. Mcwilliams, S. I. Usiskan, S. E. Pinder, M. V. Hemelrijck, and M. Douek, "Systematic review of high-intensity focused ultrasound ablation in the treatment of breast cancer," British Journal of Surgery, vol. 102, pp. 873–882, Jul. 2015.

[20] Y. You, Z. Wang, H. Ran, Y. Zheng, D. Wang, J. Xu, Z. Wang, Y. Chen, and P. Li, "Nanoparticle-enhanced synergistic HIFU ablation and transarterial chemoembolization for efficient cancer therapy," Nanoscale, vol. 8, no. 7, pp. 4324–4339, 2016.

[21] P. Zhang and T. Porter, "An in vitro Study of a Phase-Shift Nanoemulsion: A Potential Nucleation Agent for Bubble-Enhanced HIFU Tumor Ablation," Ultrasound in Medicine & Biology, vol. 36, no. 11, pp. 1856–1866, Aug. 2010.

[22] M. J. Choi, S. R. Guntur, K. I. Lee, D. G. Paeng, and A. Coleman, "A Tissue Mimicking Polyacrylamide Hydrogel Phantom for Visualizing Thermal Lesions Generated by High Intensity Focused Ultrasound," Ultrasound in Medicine & Biology, vol. 39, no. 3, pp. 439–448, 2013.

[23] A. D. Maxwell, T.-Y. Wang, L. Yuan, A. P. Duryea, Z. Xu, and C. A. Cain, "A Tissue Phantom for Visualization and Measurement of Ultrasound-Induced Cavitation Damage," Ultrasound in Medicine & Biology, vol. 36, no. 12, pp. 2132–2143, 2010.

[24] C. P. Keravnou, I. D. Cock, I. Lentacker, M.-L. Izamis, and M. A. Averkiou, "Microvascular Injury and Perfusion Changes Induced by Ultrasound and Microbubbles in a Machine-Perfused Pig Liver," Ultrasound in Medicine & Biology, vol. 42, no. 11, pp. 2676–2686, 2016.

[25] "Prostate Cancer," Focused Ultrasound Foundation, Apr-2019. [Online]. Available: https://www.fusfoundation.org/diseases-and-conditions/oncological/prostate-cancer. [Accessed: 06-May-2019].

[26] G. R. Harris, "FDA regulation of clinical high intensity focused ultrasound (HIFU) devices," Conference proceedings: ... Annual International Conference of the IEEE Engineering in Medicine and Biology Society. IEEE Engineering in Medicine and Biology Society. Annual Conference, 2009. [Online]. Available: https://www.ncbi.nlm.nih.gov/pubmed/19963452. [Accessed: 06-May-2019].

[27] "Guidelines for Ethical Conduct in the Care and Use of Nonhuman Animals in Research," Committee on Animal Research and Ethics, Feb-2012. [Online]. Available: https://www.apa.org/science/leadership/care/guidelines. [Accessed: 06-May-2019].

[28] "Requirements for measurement standards for high intensity therapeutic ultrasound (HITU) devices," IEC TR 62649:2010 , Apr-2010. [Online]. Available: https://webstore.iec.ch/publication/7320. [Accessed: 06-May-2019].

[29] K. H. Martin and P. A. Dayton, "Current status and prospects for microbubbles in ultrasound theranostics," Wiley interdisciplinary reviews. Nanomedicine and nanobiotechnology, 15-Mar-2013. [Online]. Available: https://www.ncbi.nlm.nih.gov/pmc/articles/PMC3822900/. [Accessed: 09-Jun-2019].

[30] Vignon, F., Shi, W. T., Powers, J. E., Everbach, E. C., Liu, J., Gao, S., Xie, F., & Porter, T. R. (2013). Microbubble cavitation imaging. IEEE transactions on ultrasonics, ferroelectrics, and frequency control, 60(4), 661–670. https://doi.org/10.1109/TUFFC.2013.2615

[31] Nikfarjam, Mehrdad, et al. "Mechanisms of Focal Heat Destruction of Liver Tumors." Journal of Surgical Research, vol. 127, no. 2, 2005, pp. 208–223.

[32] Dewhirst, Mark W, et al. "THERMAL DOSE REQUIREMENT FOR TISSUE EFFECT: EXPERIMENTAL AND CLINICAL FINDINGS." Proceedings of SPIE--the International Society for Optical Engineering, vol. 4954, 2003, p. 37.

[33] Heisterkamp, J, et al. "Heat-Resistant Cylindrical Diffuser for Interstitial Laser Coagulation: Comparison with the Bare-Tip Fiber in a Porcine Liver Model." Lasers in Surgery and Medicine, vol. 20, no. 3, 1997, pp. 304–309.

[34] Moritz, A R, and F C Henriques. “Studies of Thermal Injury: II. The Relative Importance of Time and Surface Temperature in the Causation of Cutaneous Burns.” The American Journal of Pathology, vol. 23, no. 5, 1947, pp. 695–720.

[35] Overmoyer, B., Mclaren, C., & Brittenham, G. (1987). Uniformity of liver density and nonheme (storage) iron distribution. Archives of Pathology & Laboratory Medicine, 111(6), 549-54.

[36] Barber, T., Brockway, J., & Higgins, L. (1970). THE DENSITY OF TISSUES IN AND ABOUT THE HEAD. Acta Neurologica Scandinavica, 46(1), 85-92.

[37] Lloyd, B. A. (n.d.). Speed of Sound. Retrieved May 6, 2020, from https://itis.swiss/virtual-population/tissue-properties/database/acoustic-properties/speed-of-sound/

[38] Fujii, Yasutomo, Taniguchi, Nobuyuki, Itoh, Kouichi, Shigeta, Kouichiro, Wang, Yi, Tsao, Jing - Wen, . . . Itoh, Takashi. (2002). A New Method for Attenuation Coefficient Measurement in the Liver. Journal of Ultrasound in Medicine, 21(7), 783-788.

[39] Taghizadehghahremanloo, S., Labuda, Cecille, Mobley, Joel, & Zhang, Likun. (2018). Development of a Tissue-mimicking Phantom of the Brain for Ultrasonic Studies, ProQuest Dissertations and Theses.

[40] Mohammad Rohani, & Alfonso Fasano. (2017). Focused Ultrasound for Essential Tremor: Review of the Evidence and Discussion of Current Hurdles. Tremor and Other Hyperkinetic Movements, 7, 462.

[41] Fishman, P., & Frenkel, S. (2017). Focused Ultrasound: An Emerging Therapeutic Modality for Neurologic Disease. Neurotherapeutics, 14(2), 393-404.

[42] Meng, Y., Suppiah, S., Surendrakumar, S., Bigioni, L., & Lipsman, N. (2018). Low-Intensity MR-Guided Focused Ultrasound Mediated Disruption of the Blood-Brain Barrier for Intracranial Metastatic Diseases. Frontiers in Oncology, 8, 338.

[43] Incionless Surgery. (1999). Retrieved from https://www.insightec.com/us

[44] W. D. O’Brien, Jr., “Ultrasound-biophysics mechanisms,” Prog. Biophys. Mol. Biol. 93, 212–255 (2007). https://doi-org.offcampus.lib.washington.edu/10.1016/j.pbiomolbio.2006.07.010

[45] Schlesinger, D., Benedict, S., Diederich, C., Gedroyc, W., Klibanov, A., & Larner, J. (2013). MR-guided focused ultrasound surgery, present and future. Medical Physics, 40(8), N/a.

[46] Cook, J., Bouchard, R., & Emelianov, S. (2011). Tissue-mimicking phantoms for photoacoustic and ultrasonic imaging. Biomedical Optics Express, 2(11), 3193-3206.

[47] OpenStax. (n.d.). Physics. Retrieved from https://courses.lumenlearning.com/physics